Electronic Supplementary Material (ESI) for Soft Matter.

Hydrogen Bonding and Charge Transport in a Protic Polymerized Ionic Liquid

Supporting Information

Arthur Markus Anton,[*,†,‡] Falk Frenzel,[†] Jiayin Yuan,[¶] Martin Tress,[§,†] and Friedrich Kremer[†]

†*Peter Debye Institute for Soft Matter Physics, Leipzig University, Linnéstraße 5, D-04103 Leipzig, Germany*

‡*Department of Physics and Astronomy, The University of Sheffield, Hicks Building, Hounsfield Road, Sheffield S3 7RH, United Kingdom*

¶*Department of Materials and Environmental Chemistry, Stockholm University, Svante Arrhenius väg 16C, SE-106 91 Stockholm, Sweden*

§*Department of Chemistry, University of Tennessee, 1420 Circle Dr., Knoxville, Tennessee 37996, USA*

E-mail: a.m.anton@outlook.de

H-Bond Sites

Possible H-bond pairs have been identified on the basis of the *Hydrogen Bond Donor/Acceptor Plugin* in Mavin by ChemAxon. Within the polymer repeat unit, the carboxyl (C=O) and the sulfite group (SO_3^-) are able to adopt the role of a hydrogen bond acceptor (Figure S1b), pronounced groups for possible donors cannot be identified. Independent of the pH value, the number of possible acceptor atoms is 4, the number of possible acceptor sites 9 (9 electron pairs, Figure S1a). In the case of hydrogen bond donors, the number of sites stays 0. In the case of the cation (Figure S1c), only the amine group (N−H) is able to donate to 1 hydrogen bond, but each of the 6 ether groups (C−O−C) is able to accept 2 bonds.

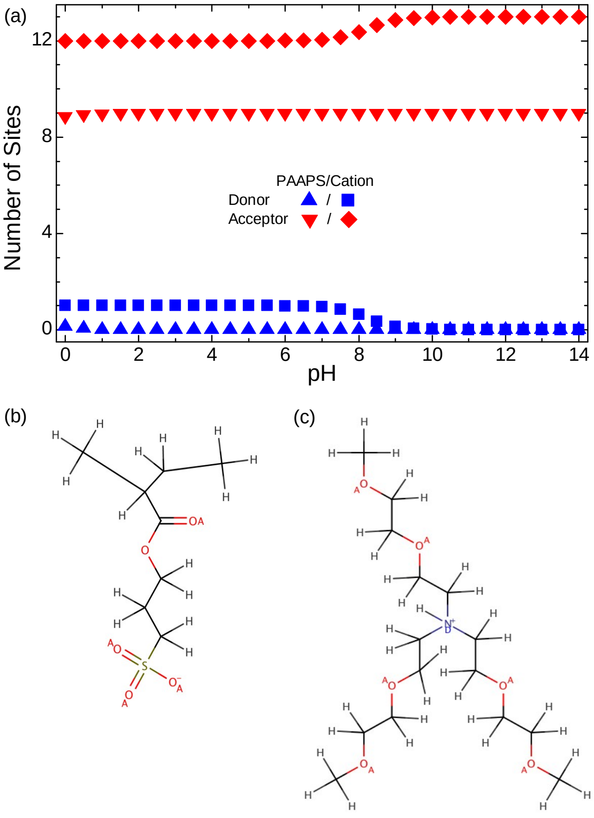

Figure S1: Possible hydrogen bond donor (D) and acceptor atoms (A) within (b) the polymer repeat unit and (c) the cation. (a) Depending on the pH value, the number of sites can slightly vary. The calculations have been performed with the *Hydrogen Bond Donor/Acceptor Plugin* in Mavin by ChemAxon.

Hysteresis and Fit of σ'

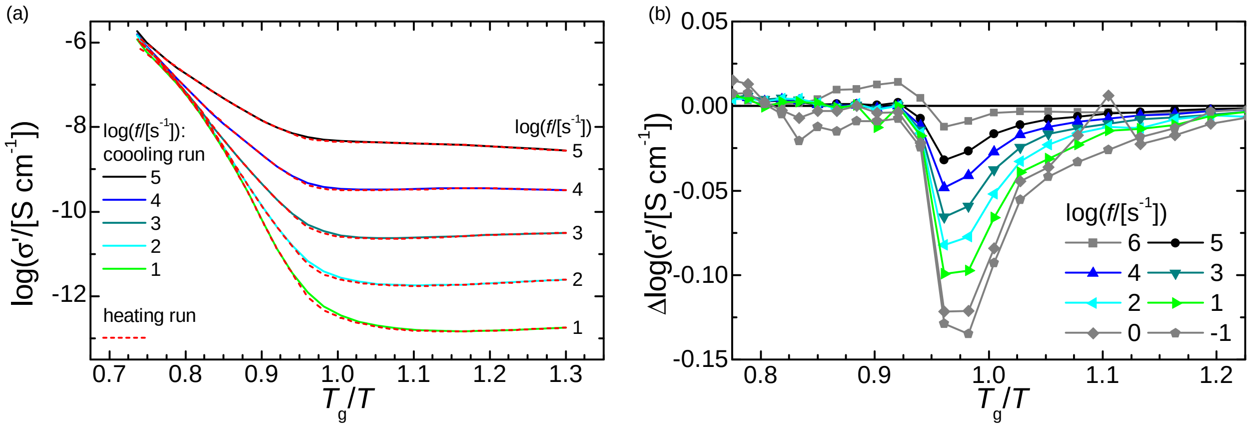

Figure S2: (a) The real part σ' of the complex conductivity function depending on the inverse temperature scaled with the glass transition temperature $T_g = 216$ K. (b) The difference between the cooling and heating run ($\Delta \log(\sigma')$). At the same temperature σ_0 is up to 20% less during heating than during previous cooling. (c) The maximum of $\Delta \log(\sigma')$ appears at 230 K.

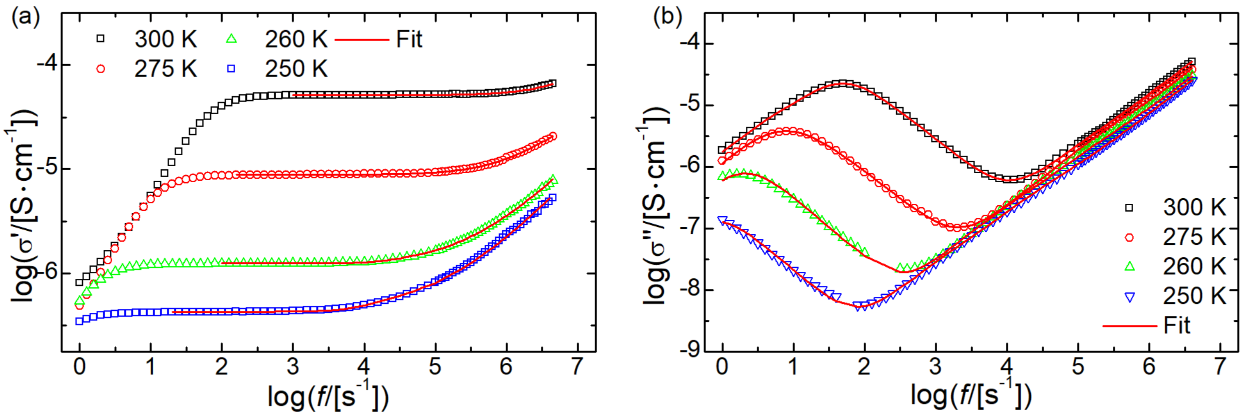

Figure S3: (a) The real part σ' and (b) the imaginary part σ'' of the complex conductivity function depending on the frequency along with fits in accord to the random free-energy barrier model.[12,13] Electrode polarization causes the plateau of σ' to bend off from the horizontal trace of the DC conductivity at low frequencies (a). Thus, these values are excluded from fitting the real part of σ^*. The rising high-frequency part of σ'' (b) is well described through the random free-energy barrier model, whereas electrode polarization is responsible for the local maximum at lower frequencies. This maximum is fitted with an additional Cole-Cole function.[14]

Spectral Assignments

In order to identify and assign molecular vibrations of the complex structure of PAAPS comparison measurements are examined using

- tris[2-(2-methoxyethoxy)ethyl]amine, TDA-1, Figure S4a
- poly(ethylene oxide), abbreviated PEO, Figure S4b
- Ethyl-2- methylbutyrate, E2MB, Figure S4c

All samples have been purchased from Sigma-Aldrich.

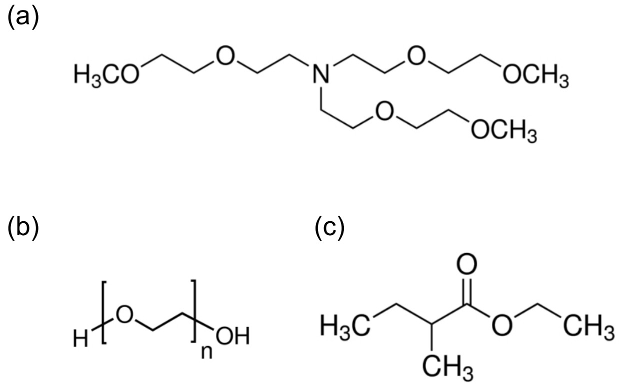

Figure S4: Materials used for comparison in order to identify peaks of PAAPS, (a) TDA-1, (b) PEO, and (c) E2MB.

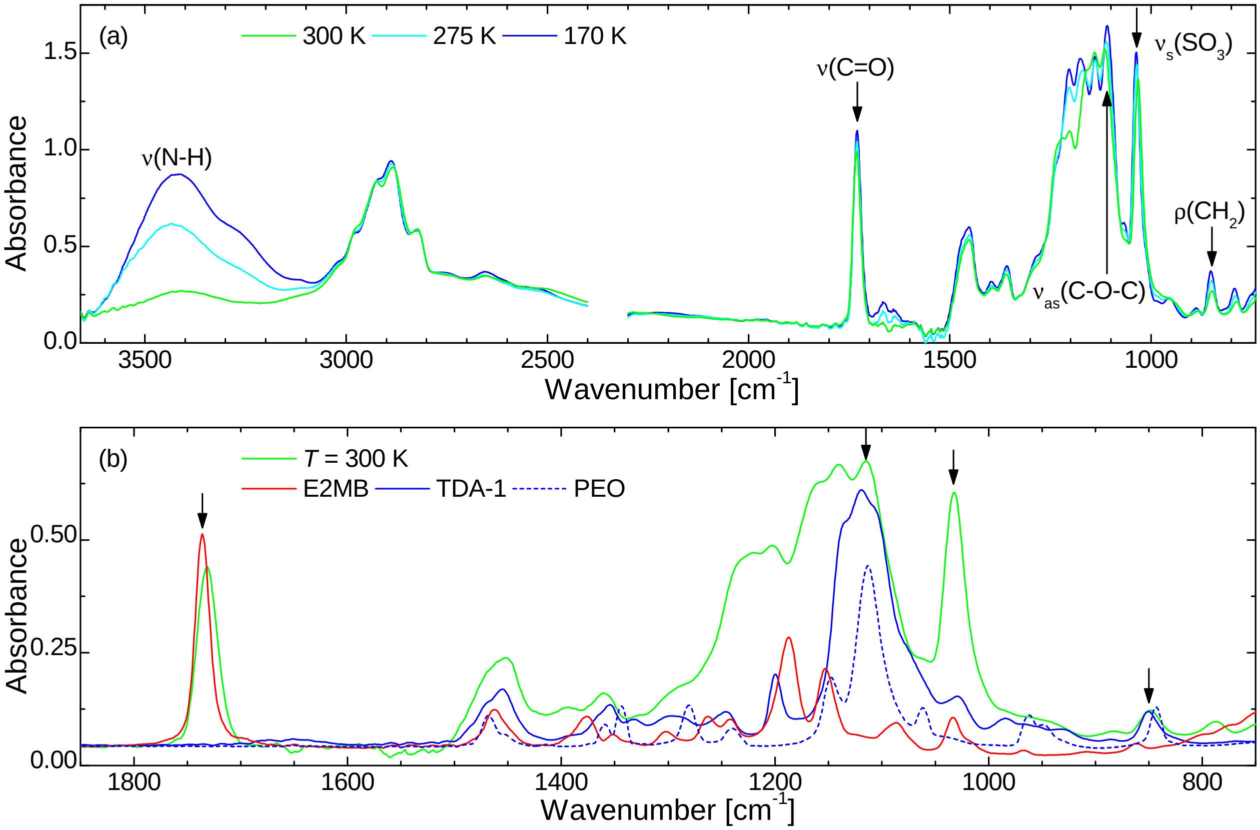

Figure S5: (a) FTIR spectra of PAAPS depending on the temperature during measurement. (b) In order to assign peaks to the distinct vibrational modes and moieties within the complex spectrum of PAAPS comparison measurements are performed.

SO_3 Stretching Vibration $\nu_{as}(SO_3)$

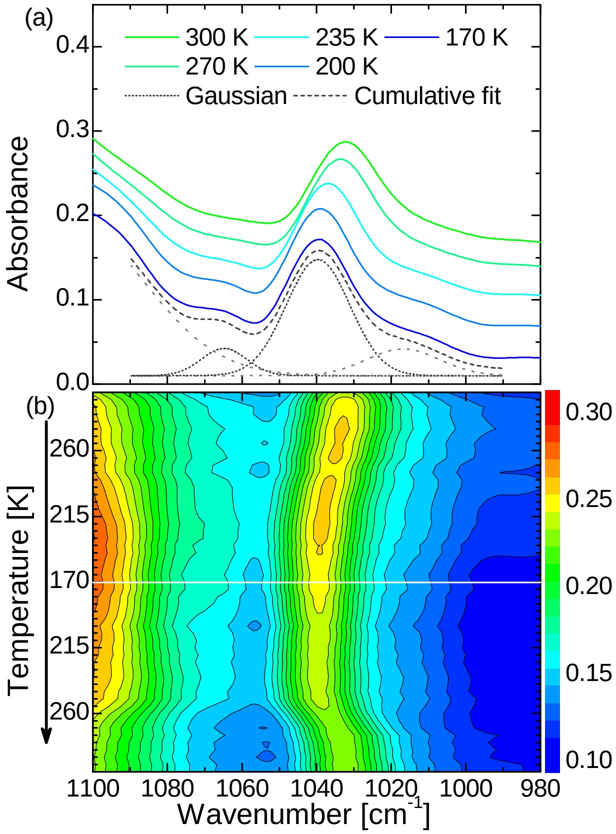

Figure S6: Temperature-dependent FTIR spectra of the spectral region around the symmetric SO_3 stretching vibration. (a) The peak, the 2 shoulders, and the adjacent band are modeled through single Gaussians; no baseline has been subtracted. For sake of clarity all spectra are shifted vertically. (b) The frequency shift is not symmetric around the lowest measured temperature (170 K, white line). The arrow at the left hand side represents the temporal sequence of measurements; the color bar at the right hand side indicates the absorbance value.

N–H Stretching Vibration $\nu\left(\text{N–H}\right)$

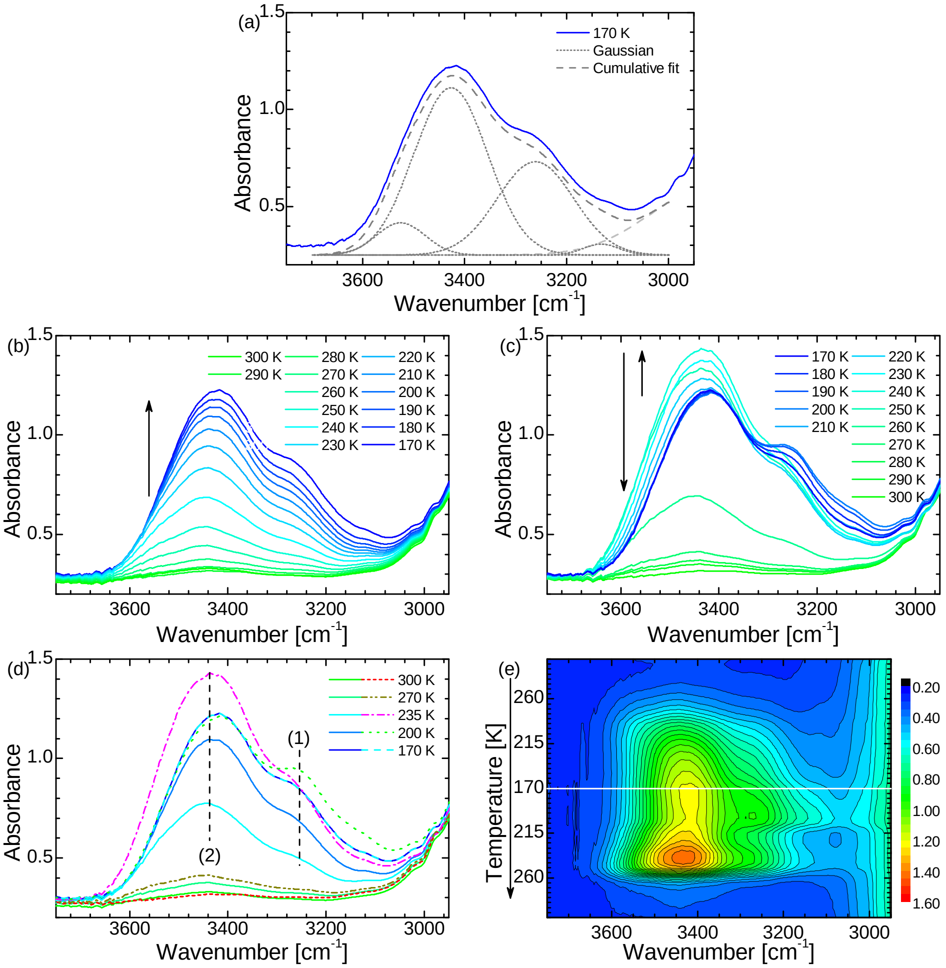

Figure S7: Temperature-dependent FTIR spectra of the spectral region around $\nu\left(\text{N}-\text{H}\right)$. (a) This band consists of 4 peaks which are modeled through Gaussians. The baseline is a polynomial function of degree 3. For sake of clarity all spectra are vertically shifted. (b) During cooling from 300 to 170 K all contributing peaks increase evenly; (c) during subsequent heating back to 300 K the peaks respond differently to the temperature increase. (d) First the absorbance of the peak at $\bar{\nu} = 3251\ \text{cm}^{-1}$ (1) rises inbetween 170 and 200 K, while the absorbance of the peak at $\bar{\nu} = 3421\ \text{cm}^{-1}$ (2) stays constant. While heating further (from 200 to 235 K) the absorbance of the peak at $\bar{\nu} = 3251\ \text{cm}^{-1}$ (1) drops, whereas the absorbance of the peak at $\bar{\nu} = 3421\ \text{cm}^{-1}$ (2) increases. For higher temperature this band decreases, because of breaking of hydrogen bonds. (e) The frequency shift is not symmetric around the lowest measured temperature (170 K, white line); the two changes in the thermal response are visible. The arrow at the left hand side represents the temporal sequence of measurements; the color bar at the right hand side indicates the absorbance value.

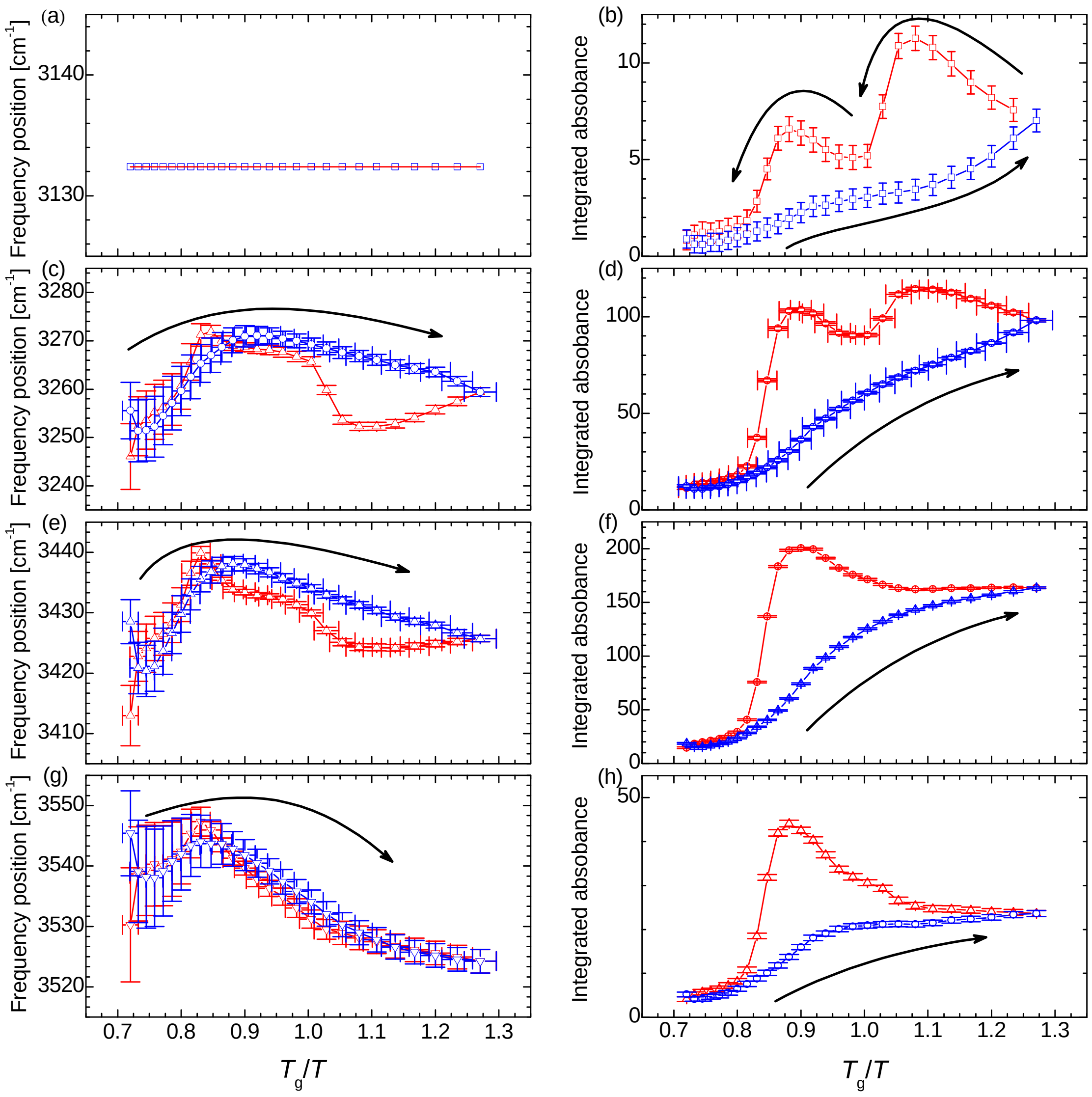

Figure S8: (a,c,e,g) Temperature-dependent frequency position and (b,d,f,h) integrated absorbance of the N−H stretching vibration $\nu\left(\mathrm{N{-}H}\right)$. The blue symbols denote data points recorded during the cooling run, the red symbols during the subsequent heating run. The arrows indicate the direction of measurement. In the case of the peak located at 3132 cm^{-1} it was mandatory to fix the *mean* peak position (after the first iteration) in order to obtain reasonable result from the fit.

C=O Stretching Vibration $\nu\left(\text{C=O}\right)$

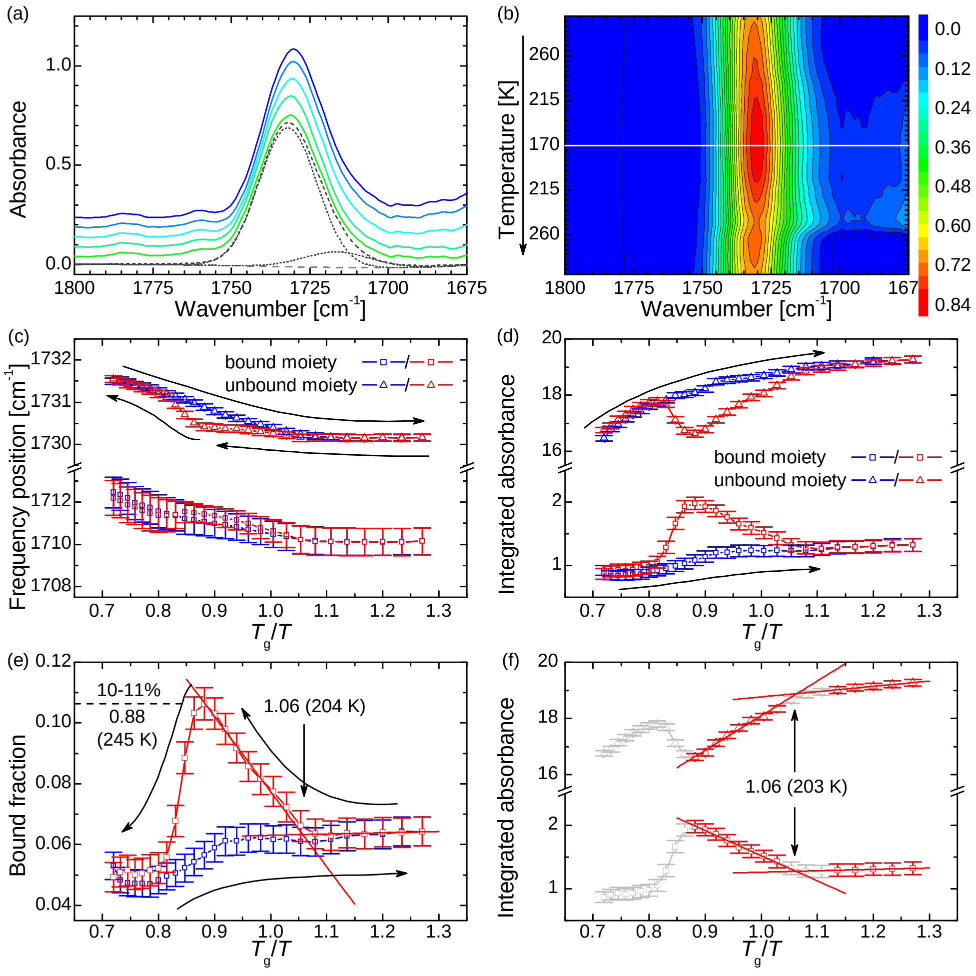

Figure S9: (a) Temperature-dependent FTIR spectra of the C=O stretching band. This band consists of two peaks from which the one at higher frequencies represents the stretching vibration of the free C=O groups, the one at lower frequencies the vibration of bound groups. (b) The frequency shift is not symmetric around the lowest measured temperature (170 K, white line). The arrow at the left hand side represents the temporal sequence of measurements; the color bar at the right hand side indicates the absorbance value. (c) The temperature-dependent frequency position and (d) integrated absorbance of $\nu\left(\text{C=O}\right)$. (e) On the basis of the integrated absorbance the fraction of bound C=O groups can be calculated (maximum value 11% at $T_g/T = 0.88$. (f) As in the case of $\nu_{as}\left(\text{SO}_3\right)$ a pronounce hysteresis is present, which sets in at $T_g/T = 1.06$. For sake of clarity all spectra are shifted vertically. The blue symbols denote data points recorded during the cooling run, the red symbols during the subsequent heating run. The arrows indicate the direction of measurement.

The C=O stretching vibration $\nu\left(\mathrm{C{=}O}\right)$ gives rise to a band around $\bar{\nu} = 1730\ \mathrm{cm}^{-1}$. It consists of two peaks ($\bar{\nu} = 1731.1\ \mathrm{cm}^{-1}$ and $\bar{\nu} = 1713.6\ \mathrm{cm}^{-1}$ at room temperature, Figure S9), from which the one at the lower frequency position represents the vibration of C=O residues incorporated into hydrogen bonding and the other at the higher frequency position the free (unbound) vibration.[1–3] On the basis of the ratio between the particular values of the integrated absorbance (represented through the area under the curve AuC) of these 2 peaks we determine the fraction of bound C=O groups $f_b\left(\mathrm{C{=}O}\right)$ in dependence of the apparent temperature.

It is not surprising that $f_b\left(\mathrm{C{=}O}\right)$ increases when the temperature is lowered; starting from 5% at 300 K $f_b\left(\mathrm{C{=}O}\right)$ adopts a value of 6% after cooling to 170 K. On the other hand, it is surprising that $f_b\left(\mathrm{C{=}O}\right)$ increases further to 11% at around $T_g/T = 0.88$ (245 K) when the sample is heated. Subsequently, $f_b\left(\mathrm{C{=}O}\right)$ reaches its initial value (Figure S9e). Similar to the case of $\nu\left(\mathrm{SO_3}\right)$, the hysteresis of $f_b\left(\mathrm{C{=}O}\right)$ sets in at $T_g/T = 1.06$ ($T =$ 204 K) in accord with the glass transition temperature of the repeat unit, not with that of the polymer. Thus, already at T_g^{RU} the side chains are mobile enough for structural reorganization. Moreover, the bound fraction is at its maximum at $T_g/T = 0.88$, which fairly coincides with the maximum difference of conductivity between cooling and heating run.

Pruthtikul et al. determined the number of hydrogen-bonding contact sites in hyperbranched polyesters forming dendrimers of generation 2 to 5 by labeling the outermost carboxyl groups.[2] Interestingly, $f_b\left(\mathrm{C{=}O}\right)$ in PAAPS is comparable with or even less than the fraction of bound carboxyl groups in the *core* of these dendrimers. Furthermore, the authors discussed that these values indicate a distinct *screening* and less accessibility of the C=O groups compared to the linear polymers of this kind. Consequently, the C=O groups in PAAPS are as well *effectively screened* which reduces the accessibility of this moiety to hydrogen bond donors similar or even less compared to polyester dendrimers.

CH_2 Rocking and C–O–C Stretching Vibration

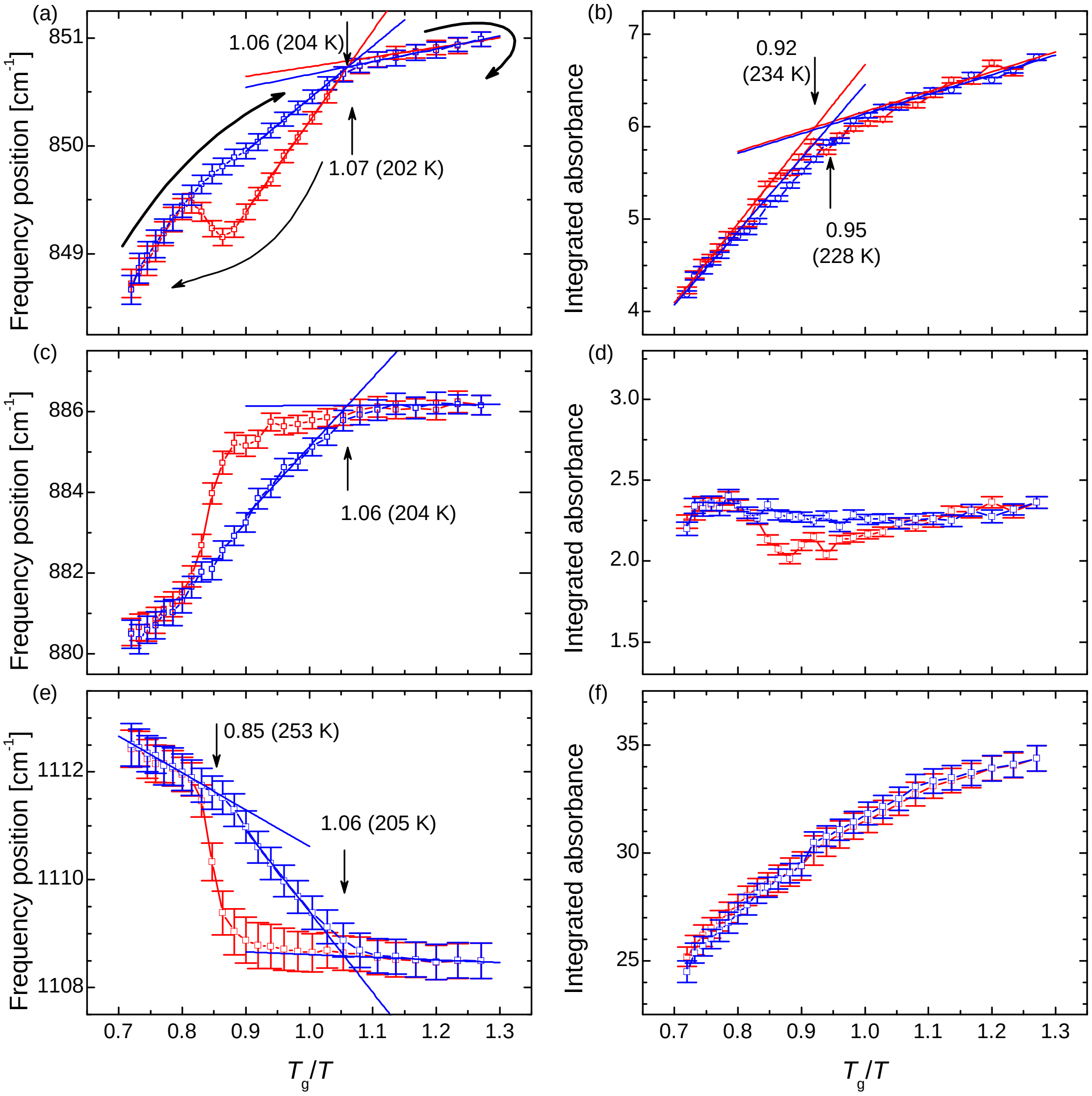

Figure S10: Temperature-dependent frequency position (a,c,e) and integrated absorbance (b,d,f) of the CH_2 rocking vibration $\rho_{\mathrm{gauche}}\,(CH_2)$ in *gauche* conformation (a,b), CH_2 rocking vibration $\rho_{\mathrm{trans-gauche}}\,(CH_2)$ at the end groups of the cation, and C−O−C antisymmetric stretching vibration $\nu_{as}\,$(C-O-C) (e,f), respectively. The blue symbols denote data points recorded during the cooling run, the red symbols during the subsequent heating run. The arrows indicate the direction of measurement. Line fits have been employed in order to extract transition points.

In addition to the H-bond acceptor moieties of the polymer and the N−H group in the cation acting as H-bond donor, the cation comprises also three arms each with two repeat units of polyethylene glycol. In order to study the structure of the whole sample we investigate as well the response of the cation arms to the temperature cycle. On the basis of comparison measurements (Figure S4 and S5) we assign the peaks around $\langle\bar{\nu}\rangle = 849\ \mathrm{cm}^{-1}$ and $\langle\bar{\nu}\rangle = 881\ \mathrm{cm}^{-1}$ to the CH_2 rocking vibration in crystalline *gauche* $\rho_{\mathrm{gauche}}\,(\mathrm{CH_2})$ and *trans-gauche* $\rho_{\mathrm{trans-gauche}}\,(\mathrm{CH_2})$ conformation of the end groups, respectively, as well as the peak at $\langle\bar{\nu}\rangle = 1115\ \mathrm{cm}^{-1}$ to the C−O−C antisymmetric stretching vibration ($\nu_{as}\left(\mathrm{C{-}O{-}C}\right)$)

When PAAPS undergoes the cooling-heating cycle, first, the frequency positions of $\rho\,(\mathrm{CH_2})$ and $\nu_{as}\left(\mathrm{C{-}O{-}C}\right)$ are reversibly shifted to higher and lower values during cooling, respectively (Figure S10a,c,e). This blue/blue shift is in full agreement with the common literature about H-bounding in which deformation/stretching vibrations in general show a blue/red upon hydrogen bond formation, respectively.[2,4,5] Second, during heating, these peaks are red and blue shifted reaching their initial values at 300 K, which demonstrates the reversibility of the origin of these spectral shifts.

Third, as before in the cases of $\nu_s\,(\mathrm{SO_3})$, $\nu\left(\mathrm{C{=}O}\right)$, and $\nu\left(\mathrm{N{-}H}\right)$ the vibration frequencies of $\rho\,(\mathrm{CH_2})$ and $\nu_{as}\left(\mathrm{C{-}O{-}C}\right)$ exhibit a clear hysteresis during the cooling-heating cycle. Despite the frequency shift of $\rho_{\mathrm{trans-gauche}}\,(\mathrm{CH_2})$ (Figure S10c,d) and $\nu_{as}\left(\mathrm{C{-}O{-}C}\right)$ (Figure S10e,f) is highly similar to the above-discussed vibrational modes (reversibility and hysteresis), the characteristic of the shift of $\rho_{\mathrm{gauche}}\,(\mathrm{CH_2})$ (Figure S10a,b) is fundamentally distinct. Whereas the two former modes exhibit a hysteresis which represents a *delay* of the reversible change (the frequency position altered because of cooling is retained during heating up to a particular temperature), the hysteresis of the latter mode, instead, represents an *acceleration* of the reversible change (the frequency shift is recovered at a lower temperature compared to the cooling run). The accelerated recovery of the frequency shift demonstrates that the temperature rate during cooling-heating cycle is sufficient for the system to follow and undergo structural reorganizations. Interestingly, the peak around $\langle\bar{\nu}\rangle = 849\ \mathrm{cm}^{-1}$ is attributed to a vibration characteristic for *crystalline* polyethyleneoxide (PEO).[6–8] Even though, Liu and Parsons mixed PEO with water or benzene , this peak remained in solution.[8]

In addition, the spectral shift of $\rho_{\text{gauche}}\left(\mathrm{CH_2}\right)$, $\rho_{\text{gauche}-\text{trans}}\left(\mathrm{CH_2}\right)$, and and $\nu_{as}\left(\mathrm{C{-}O{-}C}\right)$ bends off at $T_g/T = 1.06$ during the cooling run which is well below T_g^{Pol} but comparable to T_g^{RU}. Furthermore, for $\rho_{\text{gauche}}\left(\mathrm{CH_2}\right)$ the "accelerated" hysteresis starts at $T_g/T = 1.07$, demonstrating the local mobility of the cation sidechains below T_g^{Pol}. The expedited red shift ends at $T_g/T = 0.86$ ($T = 250$ K), where the spectral change experiences an interim blue shift until $T_g/T = 0.82$ ($T = 265$ K), before the frequency position matches the trace of the cooling run (Figure S10a). This temperature range fits with the hysteresis of $\rho_{\text{trans}-\text{gauche}}\left(\mathrm{CH_2}\right)$ and and $\nu_{as}\left(\mathrm{C{-}O{-}C}\right)$ (as well as with the hysteresis of $\nu_s\left(\mathrm{SO_3}\right)$ and $\nu\left(\mathrm{C{=}O}\right)$), where the hysteresis is passing its maximum or ends its constant trace and returns to the trace of the cooling run.

Concerning the integrated absorbance, $A_{\text{int}}\left(\rho_{\text{gauche}}\left(\mathrm{CH_2}\right)\right)$ bends of at $T_g/T = 0.95$ or 0.92 for the cooling or heating run, respectively, but does not exhibit any significant hysteresis. Thus, the number density of vibrating moieties in *gauche* conformation changes with temperature, but follows the same path during cooling and heating. This path (number density of moieties) is sensitive to T_g^{Pol}. The potential of this vibrational mode, instead, experiences a change already at T_g^{RU}. $A_{\text{int}}\left(\rho_{\text{gauche}-\text{trans}}\left(\mathrm{CH_2}\right)\right)$ is not significantly altered during the cooling-heating cycle; $A_{\text{int}}\left(\nu_{\text{as}}\left(\mathrm{C{-}o{-}C}\right)\right)$ follows a smooth trace without kinks or hysteresis.

Correlation Between Different Vibrational Modes

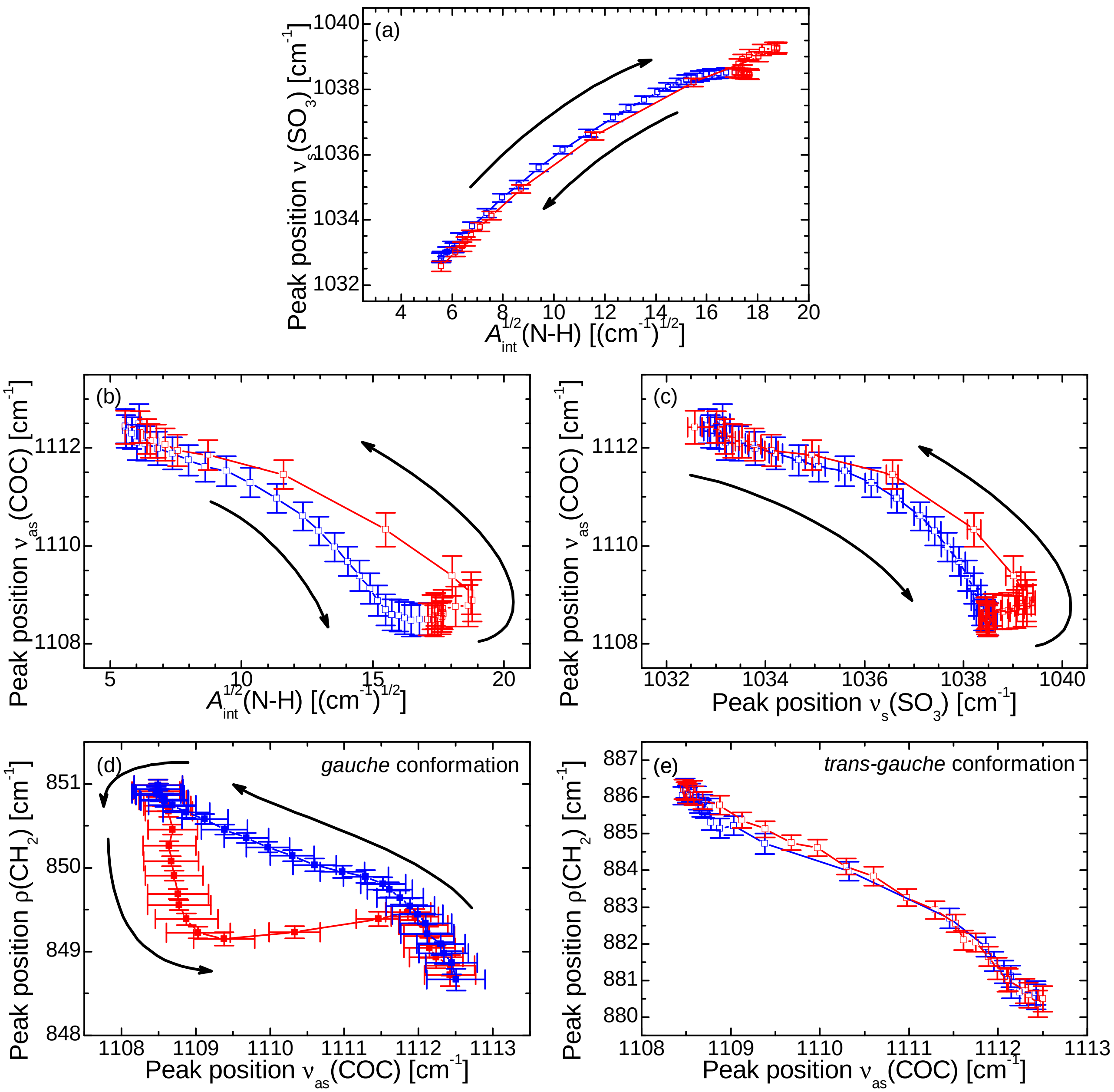

Figure S11: Correlation between the temperature-induced alterations of (a) $\nu_S\,(SO_3)$ vs. ν (N-H), (b) ν_{as} (COC) vs. ν (N-H), (c) ν_{as} (COC) vs. $\nu_S\,(SO_3)$, and (d,e) $\rho\,(CH_2)$ in *trans* and *gauche* conformation vs. ν_{as} (COC). While $\nu_S\,(SO_3)$ and ν (N-H) (a) as well as $\rho\,(CH_2)$ in *trans-gauche* conformation vs. ν_{as} (COC) show the same direct dependency on the temperature as common parameter, ν_{as} (COC) and ν (N-H) (b) as well as ν_{as} (COC) and $\nu_S\,(SO_3)$ (c) do not; ν_{as} (COC) appears constant, whereas the other vibrations are still affected by temperature change.

In order to clarify which molecular moieties are interacting with each other we prepared correlation-plots with the apparent temperature as parameter (Figure S11). Starting with the interaction between the SO_3 H-bond acceptor and N−H H-bond donor we use the linear dependence of the frequency shift and the dependence of the square root of the integrated absorbance on the hydrogen bond enthalpy.[9–11] In the according plot ($\nu_\mathrm{s}\,(SO_3)$ vs. $\nu\left(\mathrm{N{-}H}\right)^{1/2}$, Figure S11a) the individual data points representing different temperatures during the cooling and heating run form one line. Thus, we can conclude that the H-bonds are mainly formed between the SO_3 moiety of the polymer side chain and the NH group of the anion. The hysteresis during the heating run is evident as point clout coinciding with the line of points.

When we employing the same linear relation for frequency shift and square root relation for the integrated absorbance, we can exclude a significant contribution from hydrogen bonding between the free electron pairs of the C−O−C moiety within the arms of the anion and the N−H group (Figure S11b) as well as significant interactions between the C−O−C part and the SO_3 group (Figure S11c). In both scenarios the frequency shift of $\nu_{as}\,((\text{C-O-C}))$ already saturates, while the integrated absorbance of $\nu\left(\mathrm{N{-}H}\right)$ is still rising or the frequency of $\nu_\mathrm{s}\,(SO_3)$ is still shifting. Both processes indicate H-bonding while $\nu_{as}\,((\text{C-O-C}))$ is no longer affected, forming a loop in the plots. However, such interactions cannot be completely excluded; nevertheless, a significant contribution from the C−O−C parts will exclude the fairly straight line in $\nu_\mathrm{s}\,(SO_3)$ vs. $\nu\left(\mathrm{N{-}H}\right)^{1/2}$ as present.

When focusing on the rocking vibrations, it is evident that $\rho_\mathrm{gauche}\,(CH_2)$ (around $\langle\bar{\nu}\rangle =$ 849 $\mathrm{cm^{-1}}$) does not significantly interact with C−O−C moieties. While $\rho_\mathrm{gauche}\,(CH_2)$ is changing its frequency position during the heating run, $\nu_\mathrm{as}\left(\mathrm{C{-}O{-}C}\right)$ is constant (vertical trace in Figure S11d); afterward $\nu_\mathrm{as}\left(\mathrm{C{-}O{-}C}\right)$ experiences a frequency shift.

In the case of the rocking vibration of the end groups in trans-gauche conformation $\rho_\mathrm{trans-gauche}\,(CH_2)$ (around $\langle\bar{\nu}\rangle = 881\ \mathrm{cm^{-1}}$), a clear relation between frequency sifts of the particular moieties is evident. Thus, we can state that the end groups of the anion arms interact via hydrogen bonding with the free electron pair of the C−O−C moieties, giving rise to the approximately linear correlation $\rho_{\text{trans-gauche}}\,(\mathrm{CH_2})$ vs. $\nu_{as}\left(\mathrm{C{-}O{-}C}\right)$ (Figure S11e) .

Comparison between samples of different molecular weight

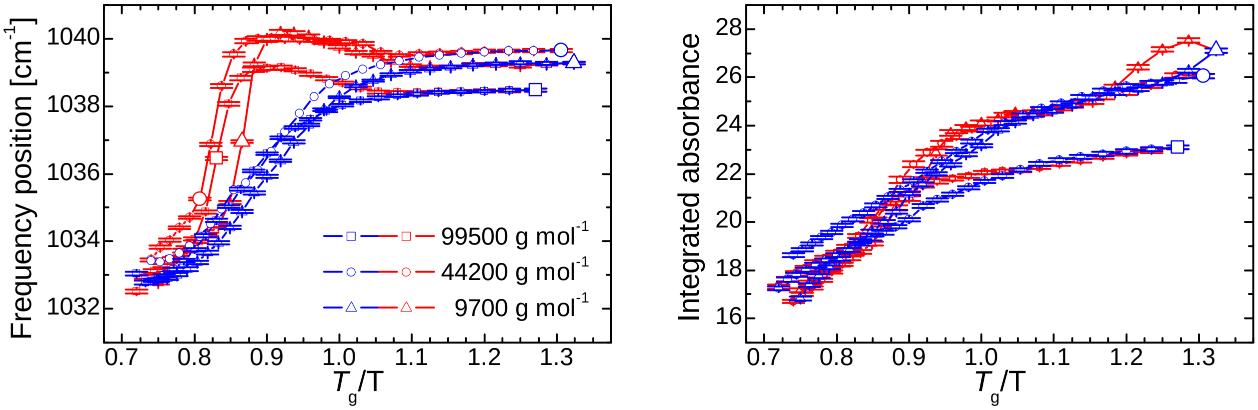

Figure S12: Frequency position $\bar{\nu}$ (left) and integrated absorbance A_{int} (right) of the symmetric SO_3 stretching vibration $\nu_s\,(SO_3)$. The blue and red symbols denote data recorded during the cooling run from 300 K to $170(K)$ and the reversed heating run, respectively. Even though the molecular weight is altered by a factor of 10, trends like the blue shift and the hysteresis are preserved. In the case of A_{int} different film thicknesses are responsible for slightly different quantitative values. However, qualitative results are not affected.

^{1}H-NM Spectroscopy on PAAPS and AAPS

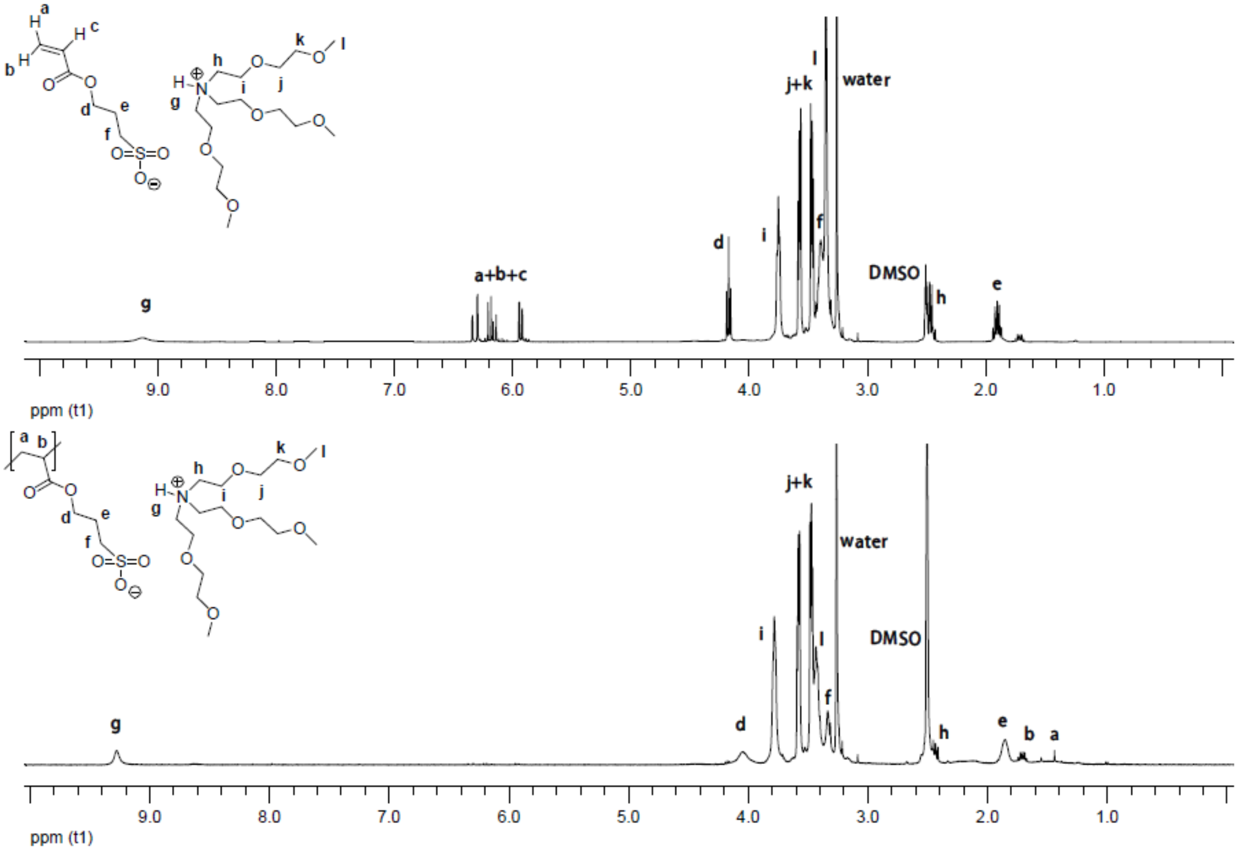

Figure S13: ^{1}H-NMR spectra of the IL repeat unit AAPS and the polyIL PAAPS in DMSO-d_6.

References

(1) Coleman, M. M.; Pehlert, G. J.; Painter, P. C. Functional Group Accessibility in Hydrogen Bonded Polymer Blends. Macromolecules **1996**, 29, 6820–6831

(2) Pruthtikul, R.; Coleman, M. M.; Painter, P. C.; Tan, N. B. Screening Effects in Solutions of a Hyperbranched, Dendrimer-Like Polyester. Macromolecules **2001**, 34, 4145–4150

(3) Mikhaylova, Y.; Adam, G.; Häussler, L.; Eichhorn, K.-J.; Voit, B. Temperature-dependent FTIR spectroscopic and thermoanalytic studies of hydrogen bonding of hydroxyl (phenolic group) terminated hyperbranched aromatic polyesters. Journal of Molecular Structure **2006**, 788, 80 – 88

(4) Desiraju, G. R.; Steiner, T. The Weak Hydrogen Bond In Structural Chemistry and Biology; IUCr Monographs on Crystallographys; Oxford University Press, 2001

(5) Steiner, T. The Hydrogen Bond in the Solid State. Angewandte Chemie International Edition **2002**, 41, 48–76

(6) Dissanayake, M. A. K. L.; Frech, R. Infrared Spectroscopic Study of the Phases and Phase Transitions in Poly(ethylene oxide) and Poly(ethylene oxide)-Lithium Trifluoromethanesulfonate Complexes. Macromolecules **1995**, 28, 5312–5319

(7) Yoshihara, T.; Tadokoro, H.; Murahashi, S. Normal Vibrations of the Polymer Molecules of Helical Conformation. IV. Polyethylene Oxide and Polyethylene-d4 Oxide. The Journal of Chemical Physics **1964**, 41, 2902–2911

(8) Liu, K.-J.; Parsons, J. L. Solvent Effects on the Preferred Conformation of Poly(ethylene glycols). Macromolecules **1969**, 2, 529–533

(9) Drago, R. S.; O'Bryan, N.; Vogel, G. C. A frequency shift-enthalpy correlation for a given donor with various hydrogen-bonding acids. J. Am. Chem. Soc. **1970**, 92, 3924–3929

(10) Ioganssen, A. Direct proportionality of the hydrogen bonding energy and the intensification of the stretching ν(XH) vibration in infrared spectra. Spectrochim. Acta Part A: Mol. Biomol. Spectros. **1999**, 55, 1585–1612

(11) Zhang, Q.-G.; Wang, N.-N.; Yu, Z.-W. The Hydrogen Bonding Interactions between the Ionic Liquid 1-Ethyl-3-Methylimidazolium Ethyl Sulfate and Water. J. Phys. Chem. B **2010**, 114, 4747–4754

(12) Dyre, J. C. The random free-energy barrier model for ac conduction in disordered solids. J. Appl. Phys. **1988**, 64, 2456–2468

(13) Schröder, T. B.; Dyre, J. C. Scaling and Universality of ac Conduction in Disordered Solids. Phys. Rev. Lett. **2000**, 84, 310–313

(14) Kremer F.; Schönhals A.; Eds. Broadband Dielectric Spectroscopy, Springer, Berlin **2000**

(15) Halgren, T. A. Merck molecular force field. I. Basis, form, scope, parameterization, and performance of MMFF94. J. Comput. Chems. **1996**, 17, 490—519